

SITULA EMT09/554.665 – TIN BRONZE – IRON AGE – SWITZERLAND

Artefact name	Situla EMT09/554.665
Authors	Christian. Degriigny (HE-Arc CR, Neuchâtel, Neuchâtel, Switzerland) & Marie-Jeanne. Scholl (HE-Arc CR, Neuchâtel, Neuchâtel, Switzerland) & Valentin. Boissonnas (HE-Arc CR, Neuchâtel, Neuchâtel, Switzerland)
Url	/artefacts/902/

✖ The object

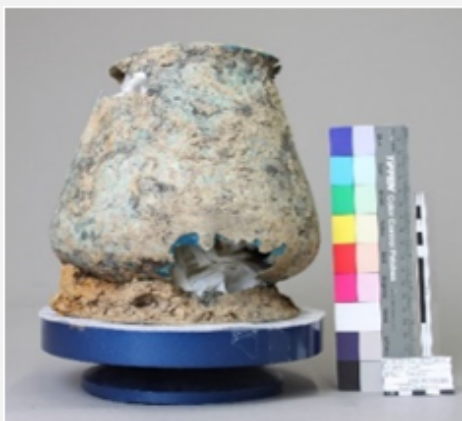


Fig. 1: Situla (Archeodunum (Gollion), 2009) inverted as found in situ,

Credit HE-Arc CR, M.-J.Scholl.

✖ Description and visual observation

Description of the artefact	Situla (Fig. 1) covered with blue-green corrosion products and sediments. Attached to two riveted iron loops is an iron handle terminating in two swan heads (not shown here). Dimensions of the main body: Hmax = 340mm, Ømax = 220mm.
Type of artefact	Situla
Origin	Mormont sanctuary, La Sarraz, Vaud, Switzerland
Recovering date	Excavated in 2011
Chronology category	Iron Age
chronology tpq	140 B.C. ▼
chronology taq	30 B.C. ▼
Chronology comment	La Tène D

Burial conditions / environment	Soil
Artefact location	Musée cantonal d'archéologie et d'histoire, Lausanne, Vaud
Owner	Musée cantonal d'archéologie et d'histoire, Lausanne, Vaud
Inv. number	EMT09/554.665
Recorded conservation data	N/A

Complementary information

The size and quality of the object makes it likely that is was reserved for important occasions or for ritual use. Secondary use could be a votive offering. Burial condition: inside a 3 meters deep hole in upside-down position.

Study area(s)

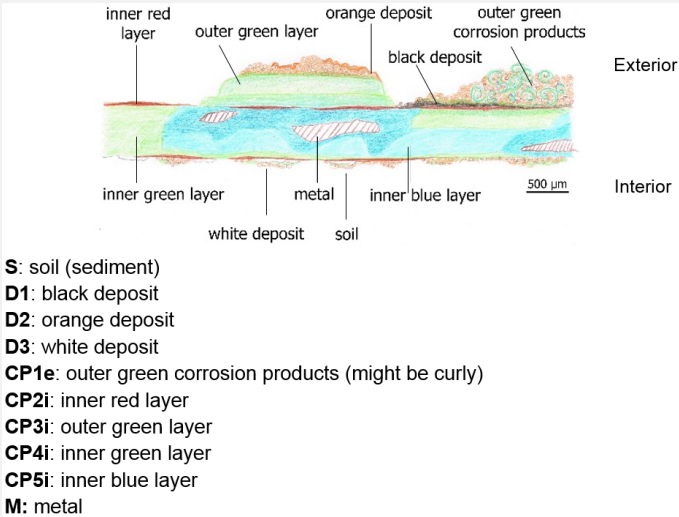


Credit HE-Arc CR, M-J.Scholl.

Fig. 2: Location of sampling area and sample selected from detached fragments,

Binocular observation and representation of the corrosion structure

The schematic representation below gives an overview of the corrosion layers encountered on the situla from a first visual macroscopic observation (additional e and i within the coding correspond to strata in contact with the environment (e) and internal strata (i)).



Credit HE-Arc CR, M-J.Scholl.

Fig. 3: Stratigraphic representation of the situla by macroscopic observation,

✧ MiCorr stratigraphy(ies) – Bi

✧ Sample(s)

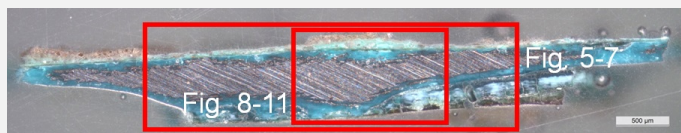


Fig. 4: Micrograph of the cross-section of the sample taken from the detached fragment of the situla showing the location of Figs. 5 to 7, 8 to 11. Unetched, dark field, 50x,

Credit HE-Arc CR, M-J.Scholl.

Description of sample

The sample was cut from a detached fragment of the upper part of the main body of the situla in Fig. 2. The cross-section is representative of the entire thickness (0.5 mm) of the object's body where on the outside there is a thicker accumulation of corrosion including curly malachite (?) clusters (Fig. 3). A metallic core is still present inside the corrosion products layers (Fig. 4).

Alloy

Tin Bronze

Technology

Cold worked (hammering on a counter-mould), annealed but no final annealing

Lab number of sample

None

Sample location

HE-Arc CR, Neuchâtel, Neuchâtel

Responsible institution

Musée cantonal d'archéologie et d'histoire, Lausanne, Vaud

Date and aim of sampling

2014, metallography and chemical analyses (FTIR, SEM-EDS)

Complementary information

None.

✧ Analyses and results

Analyses performed:

Metallography (etched with ferric chloride reagent), SEM-EDS, FTIR, Raman spectroscopy and XRD.

✧ Non invasive analysis

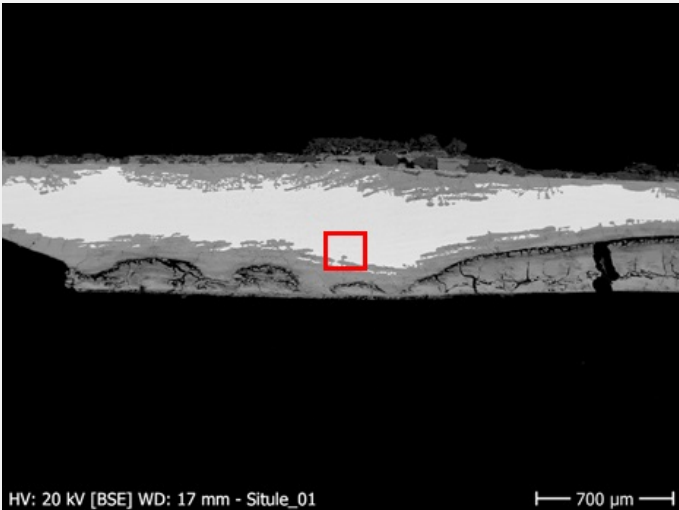
None.

✧ Metal

The remaining metal is a dense tin bronze (Fig. 5, Table 1), showing no inclusion. In bright field, the etched alloy shows a structure principally consisting of polygonal alpha phase grains (Fig. 6). Some of the grains include twin lines (Fig. 7). The presence of strain lines (slip lines) indicates a final cold work without annealing.

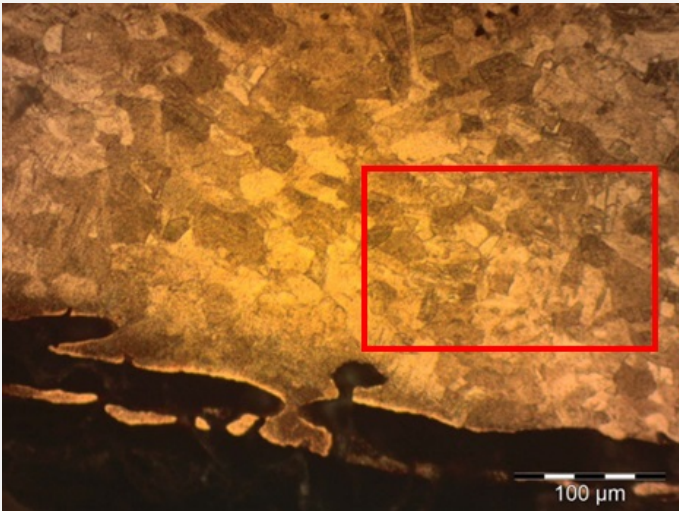
Elements	Cu	Sn
mass%	90	10

Table 1: Chemical composition of the metal. Method of analysis: SEM-EDS, Lab of Electronic Microscopy and Microanalysis, IMA (Néode), HEI Arc.



Credit HEI Arc, S.Ramseyer.

Fig. 5: SEM image, BSE-mode, of the metal sample from Fig. 4. Area of Fig. 6 is marked by a red square,



Credit HE-Arc CR.

Fig. 6: Micrograph of the metal structure from Fig. 5 (detail), etched, bright field, 50x. The alpha phase of the alloy shows polygonal grains. Area of Fig. 7 is marked by a red rectangle,

Fig. 7: Micrograph of the selected area of Fig. 6, etched, bright field, 500x. The grains show both twin and strain lines,



Credit HE-Arc CR.

Microstructure	Polygonal grain with twin and strain lines
First metal element	Cu
Other metal elements	Sn

Complementary information

None.

Corrosion layers

The corrosion crust is heterogeneous and has in places completely replaced the metal. The metal – corrosion products interface is irregular due to transgranular corrosion (Figs 5-6). In most cases, the corrosion crust can be divided in three main layers: first, an inner compact blue layer directly on the metal core (CP5, Figs. 8, 10 and 15 and CP3, Fig. 14). In areas of extensive corrosion this blue layer coexists with a friable light blue-green layer (CP4, Figs. 8, 10 and 15 and CP2, Fig. 14). Secondly, and depending on the area, either a very fine dark green (CP3, Figs. 8 and 15) or red corrosion layer (CP2, Figs. 10 and 15) marks the limit of the original surface. Finally, there is a fourth outer layer, consisting of friable and sometimes curly pale green corrosion products, interspersed with soil products (CP1, Figs. 8, 10 and 15). In heavily worked and fragile parts of the object a cleavage between the inner layers of blue and light blue-green corrosion is present, rendering the light blue-green corrosion vulnerable to loss (Fig. 9).

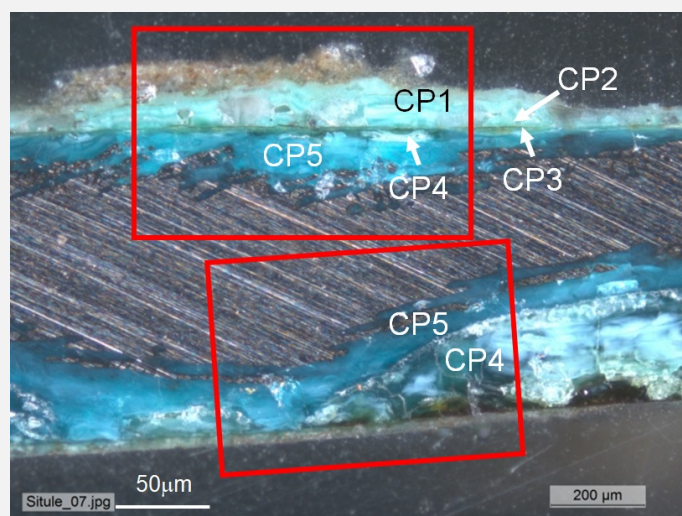
There are 2 stratigraphies (Fig. 14 corresponding to the interior face of the situla and Fig. 15 to its exterior face). The strata are similar in composition but their coding is different: CP1 to CP3 in Fig. 14 correspond to CP3 to CP5 in Fig. 15. Since the stratigraphy of Fig. 15 is more complete, the composition of each of its strata is given below.

The inner layers (CP3-CP5) are Sn and O-rich and depleted in Cu (Table 2). The outer layers (CP1 and CP2) are Cu and O-rich, contain no Sn, and are contaminated with Ca, Si, Al and Fe coming from the soil (Fig. 11). The colour of the corrosion crust varies according to the content of Sn (the more Sn, the darker green or blue the corrosion). FTIR on the inner blue (CP5 and Fig. 12) and outer green (CP1 and Fig. 13) layers were difficult to interpret. Only malachite could be identified in both cases. XRD spectra could not be interpreted because of the deficiency of peaks.

The limit of the original surface is well defined (interface of CP1 and CP2) but due to the fragility of the inner corrosion layers it was difficult to uncover.

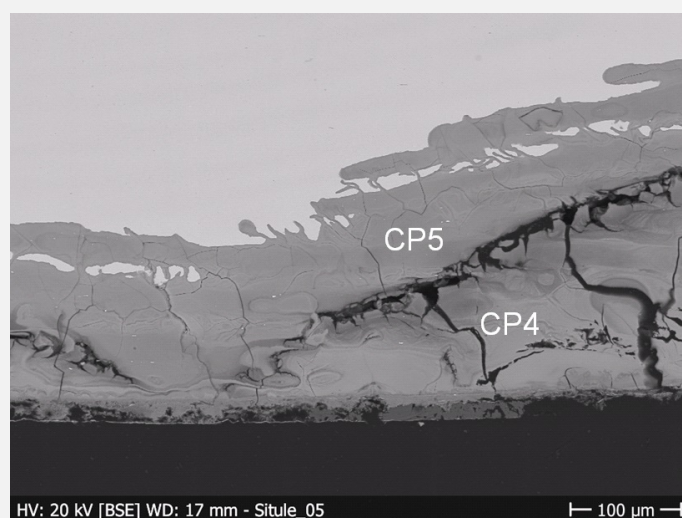
Elements	O	Cu	Sn
Outer green layer (CP1)	+++	+++	nd
Inner light blue-green layer (CP4)	++	+	+++
Inner blue layer (CP5)	++	+	+++
Remnant metal phase	nd	+++	+

Table 2: Chemical composition of the corrosion crust from Fig. 10. SEM-EDS, Lab of Electronic Microscopy and Microanalysis, IMA (Néode) (+++: high concentration, ++ medium concentration, + low concentration, nd: not-detected).



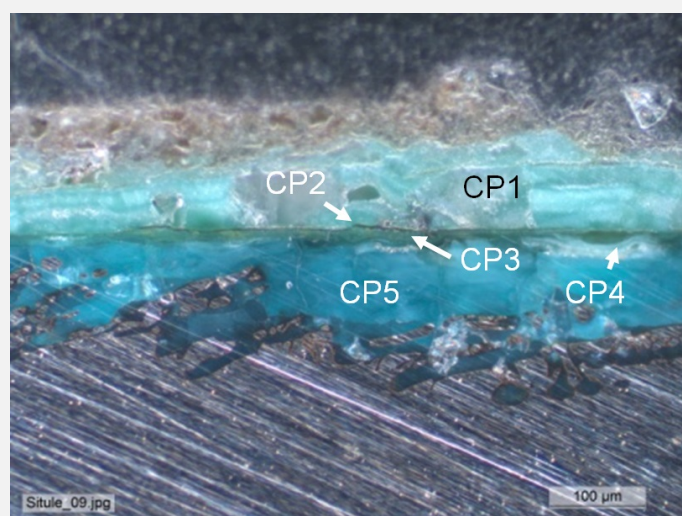
Credit HE-Arc CR.

Fig. 8: Micrograph of the metal sample from Fig. 4, unetched, dark field, 50x. Areas of Fig. 9 (bottom, corresponding to the stratigraphy of Fig. 14) and Figs. 10 and 11 (top, corresponding to the stratigraphy of Fig. 15) are marked by a rectangle. Codes are those of Fig. 15,



Credit HEI Arc, S.Ramseyer.

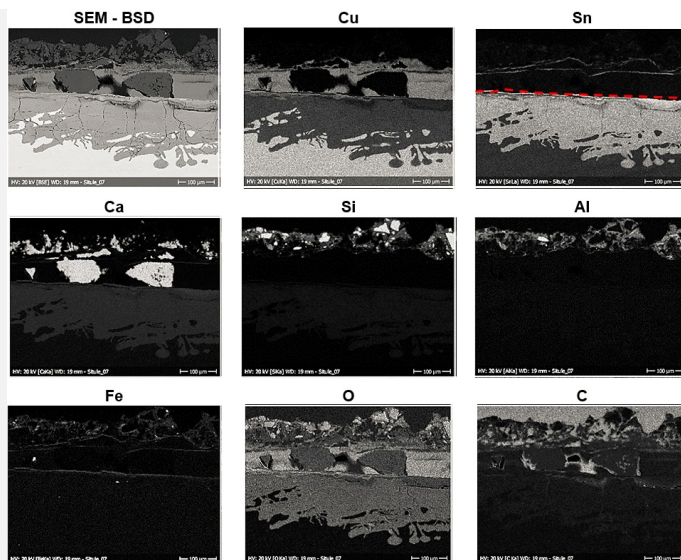
Fig. 9: SEM image, BSE-mode of the metal sample from Fig. 8 (detail) showing cleavage between the inner blue (CP5) and green (CP4) layers of Fig. 15,



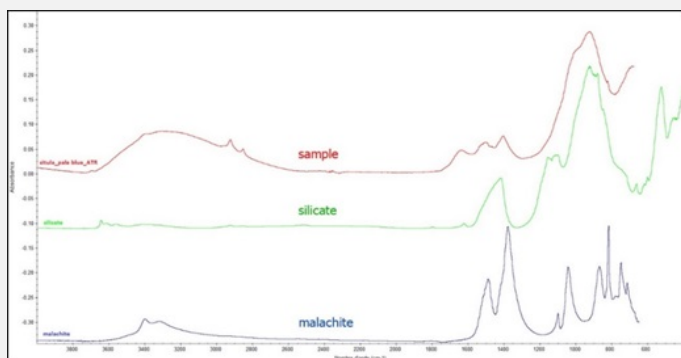
Credit HE-Arc CR.

Fig. 10: Micrograph of the metal / corrosion interface (detail of Fig. 8) unetched, dark field, 100x. The outer layer (CP1 of Fig. 15) incorporates soil material and the thin dark layer (CP2 of Fig. 15) highlights the limit of the original surface,

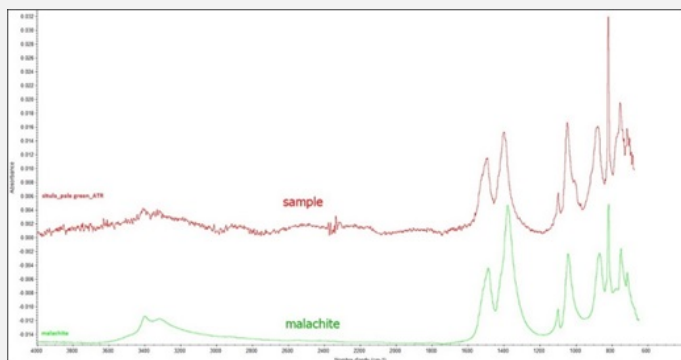
Fig. 11: SEM image, SE-mode, and elemental chemical distribution of Fig. 10. In red: the limit of the original surface highlighted by the enriched tin layer. Method of examination: SEM-EDS, Lab of Electronic Microscopy and Microanalysis, IMA (Néode), HEI Arc,



Credit HEI Arc, S.Ramseyer.



Credit HE-Arc CR.



Credit HE-Arc CR.

Corrosion form

Multiform - transgranular

Corrosion type

Type I (Robbiola)

Complementary information

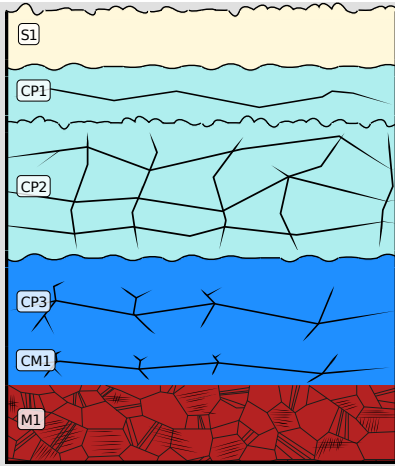
None.

✎ MiCorr stratigraphy(ies) – CS

Fig. 12: FTIR spectrum (ATR mode) of the inner blue layer (CP5) compared to the silicate and malachite standard spectrum. Method of analysis: FTIR spectroscopy, HE- Arc CR,

Fig. 13: FTIR spectrum (ATR mode) of the outer green layer (CP1) compared to the malachite standard spectrum. Method of analysis: FTIR spectroscopy, HE-Arc CR,

Fig. 14: Stratigraphic representation of the sample taken from the detached fragment of the situla in cross-section (dark field) using the MiCorr application. The characteristics



of the strata are only accessible by clicking on the drawing that redirects you to the search tool by stratigraphy representation. This representation shows the interior face and can be compared to Fig. 8 (bottom red rectangle), Credit HE-Arc CR, M-J.Scholl.

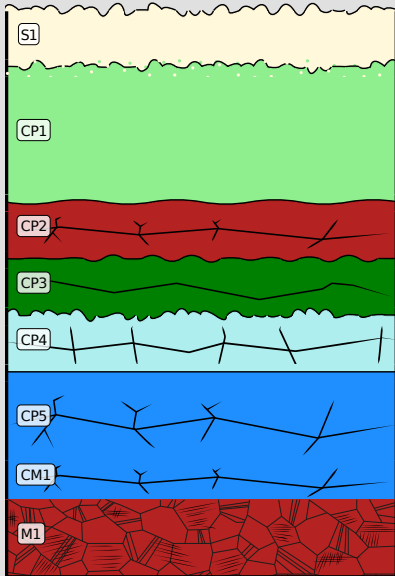


Fig. 15: Stratigraphic representation of the sample taken from the detached fragment of the situla in cross-section (dark field) using the MiCorr application. The characteristics of the strata are only accessible by clicking on the drawing that redirects you to the search tool by stratigraphy representation. This representation shows the exterior face and can be compared to Fig. 8 (top red rectangle), Credit HE-Arc CR, M-J.Scholl.

✎ Synthesis of the binocular / cross-section examination of the corrosion structure

The schematic representation of corrosion layers of Fig. 3 integrating additional information (e and i within the coding correspond to strata in contact with the environment (e) and internal strata (i)) based on the analyses carried out is given in Fig. 16.

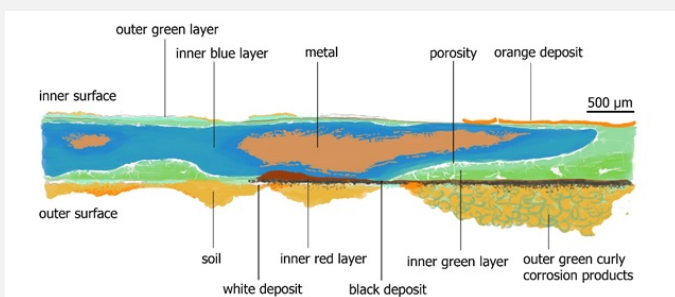


Fig. 16: Improved stratigraphic representation of the situla from visual observations and analyses,

Strata	Composition
Soil (S)	Ca, Si, Al, Fe
Black deposit (D1)	C
Orange deposit (D2)	Ferrous oxides
White deposit (D3)	Ca
Outer green curly corrosion product (CP1e)	Copper carbonates (curly malachite)
Inner red (CP2i)	Copper oxide (cuprite ?)
Outer green layer (CP3i)	Copper carbonates (malachite)
Inner green layer (CP4i)	Copper carbonates (?) + Sn
Inner blue layer (CP5i)	Copper carbonates (?) + Sn
Remnant metal phase (M)	Bronze (90%Cu, 10% Sn)

✧ Conclusion

The metal structure of this low-tin bronze shows extensive cold work and multiple annealing cycles with a final cold work. The total absence of inclusions highlights a highly developed knowledge in bronze metallurgy. The metal is much corroded. Transgranular corrosion is visible. The majority of the internal corrosion products are composed of copper carbonates that have replaced much of the metal. Curly malachite has developed in clusters on the outside of the surface. This pattern is characteristic of a long-term burial period. The presence of inner enriched Sn layers shows a decuprification phenomenon (dissolution of Cu). Because of the friable nature of the inner blue-green layer that supports the limit of the original surface, as well as its cleavage with the blue layer underneath, the original surface has become very fragile. The corrosion is thought to be of type 1 according to Robbiola et al. 1998.

✧ References

References on object and sample

Reference object

1. Archeodunum (Gollion) (2009) Le Mormont : un sanctuaire des Helvètes en terre vaudoise vers 100 avant J.-C. Section de l'archéologie cantonale, Lausanne.

Reference sample

2. Scholl, M-J. (2013) Situle en bronze et anse en fer, EMT09/554.665, vers 100 av. J.-C., La Sarraz/Eclépens, Le Mormont (VD), Musée cantonal d'archéologie et d'histoire, Lausanne. Rapport d'intervention, Haute Ecole Arc de Conservation-restauration, Neuchâtel [not published].

3. Eggert, G. (2007) Pseudomorph or corrosion? The enigma of the curly malachite, in Metal07 - Proceedings of the International Conference on Metals Conservation, Degriigny, C., Van Langh, R., Ankersmit, B. and Joosten, I. (eds), Rijksmuseum, Amsterdam, 1, 57-60.

References on analytic methods and interpretation

4. Robbiola, L., Blengino, J-M., Fiaud, C. (1998) Morphology and mechanisms of formation of natural patinas on archaeological Cu-Sn alloys, Corrosion Science, 40, 12, 2083-2111.